Title

Advancing the helox compensation method to estimate intercellular humidity in leaves of diverse species

Journal

New Phytologist

ISSN

0028-646X

Authors

Jolly, Amber R

Buckley, Thomas N

Publication Date

2026-09-13

DOI

10.1111/nph.71584

Advancing the helox compensation method to estimate intercellular humidity in leaves of diverse species

Amber R. Jolly and Thomas N. Buckley*

Department of Plant Sciences, University of California, Davis, CA 95616

*corresponding author (tnbuckley@ucdavis.edu)

0000-0002-7330-1950 (ARJ), ORCID: 0000-0001-7610-7136 (TNB)

Heading: A 4th experimental method confirms leaf airspace unsaturation, from 71-94%, in eight species

Social media handles: @tombuckleylab.bsky.social, @ucdavisplants.bsky.social

Graphical abstract: please use Figure 3

Summary

Research conducted. The relative humidity in the intercellular airspaces of leaves (*h*) has long been thought to be saturating, but several recent studies have questioned this assumption. We present, develop and demonstrate a method to estimate *h*, describe practical considerations for its application, and demonstrate it on eight species (*Gossypium hirsutum, Helianthus annuus, Heteromeles arbutifolia, Laurus nobilis, Liriodendron tulipifera, Magnolia grandiflora, Oryza sativa*, and *Pyrrosia hastata*).

Methods. N_2/O_2 (nitox) is replaced with He/O_2 (helox), which speeds stomatal diffusion, but ambient humidity is simultaneously increased to keep transpiration rate unchanged. Setting equal the expressions for transpiration in nitox and helox leads to a solution for *h*.

Key Results. We were able to rapidly switch to helox and simultaneously change humidity such that transpiration rate remained unchanged to within ± 2.5% (< 0.54% in most cases). We found *h* ranging between 71 and 94% of saturation.

Conclusion. Whereas other methods to estimate *h* either require special analytical tools (isotopic gas analysis, spectroscopically resolved fluorescence measurements with proprietary fluorophores) or special conditions (amphistomatous broad leaves with zero CO_2 exchange at one leaf surface), our method requires only water vapor concentration measurements and can be performed on any leaf under nearly any conditions.

keywords: unsaturation, stomatal conductance, transpiration, nitox, Gaastra, subsaturation

Introduction

Leaf photosynthesis and transpiration are strongly governed by the diffusive conductance between the leaf's intercellular airspaces and the ambient environment (total conductance to water vapor, g_{tw}). g_{tw} is operationally defined in relation to transpiration rate (E; symbols defined in Table 1) and the water vapor mole fractions in the ambient air (w_a) and the intercellular airspaces ($w_i = hw_s$, where w_s is the saturated value and h is intercellular relative humidity):

$$E = \frac{g_{tw}(hw_s - w_a)}{1 - \frac{1}{2}(hw_s + w_a)}. \quad (1)$$

Because w_i cannot be measured directly, g_{tw} is traditionally estimated by assuming the intercellular airspaces are saturated, i.e., $w_i = w_s$ ($h = 1$), based on early experiments consistent with this assumption (Gaastra, 1959; Farquhar & Raschke, 1978). Stomatal conductance to water vapor (g_{sw}) is then estimated from g_{tw} using estimates for boundary layer and cuticular conductances to water vapor (Caemmerer & Farquhar, 1981). Thus, nearly all experimental measurements of stomatal conductance and its responses to the environment for the past half-century are laden with the assumption that $h = 1$. Moreover, because intercellular CO_2 mole fraction (c_i) is estimated from g_{sw}, it follows that nearly all experimental measurements that depend on c_i – including parameters of photosynthetic models fitted to paired measurements of CO_2 assimilation rate (A) and c_i, and most estimates of mesophyll diffusional conductance to CO_2 – are also laden with the assumption that $h = 1$.

Several recent studies (Cernusak *et al.*, 2018; Wong *et al.*, 2022; Jain *et al.*, 2025) have presented compelling experimental evidence that challenges the assumption of saturation. Each of those studies used one of three clever experimental approaches to arrive at their conclusions: (1) The Cernusak method applies paired measurements of gas exchange and stable oxygen isotopic composition ($\delta^{18}O$) to a theoretical model, leading to two independent estimates of $\delta^{18}O$ for CO_2 at the evaporating sites, of which one depends on h; an estimate for h is then adjusted until the two $\delta^{18}O$ estimates agree. (2) The Wong method measures gas exchange independently at each surface of an amphistomatous leaf, and reduces ambient CO_2 concentration (c_a) at one surface until $A = 0$ at that surface, ensuring $c_a = c_i$ at that surface; with c_i known, one can infer g_{sw} and thus w_i. (3) The Jain method embeds water in the mesophyll apoplast with a FRET reporter ('Aquadust'; Jain *et al.*, 2021) whose fluorescence depends on local water potential; spectroscopically resolved fluorescence measurements then provide an estimate

of the water potential of the mesophyll apoplast, and hence of the relative humidity of water vapor adjacent to the apoplastic evaporating site. Each of these methods has technical limitations that limit its application: method #1 requires costly instrumentation to measure $\delta^{18}O$ and relies on assumptions about fractionation constants; method #2 only works on amphistomatous broad leaves, requires low c_a and $A = 0$ at one surface, and requires two independent gas exchange systems; and method #3 requires spectroscopically resolved fluorometry and access to a proprietary substance, Aquadust. Thus, while these methods have made profound scientific contributions in demonstrating the occurrence of unsaturated conditions in leaf intercellular airspaces, a method with fewer such technical restrictions would have great value. Moreover, there is also intrinsic value in providing further validation of the findings from those methods using another, independent approach.

Egorov and Karpushkin (1988; EK) proposed an alternative method, in which the nitrogen in air (nitox, 79% N_2/21 %O_2) is replaced with helium, making helox (79% He/21 %O_2). This should cause transpiration rate to increase, because vapor diffuses much faster in helox than in nitox. However, in the EK experiment, ambient humidity is increased at the same time nitox is replaced with helox, which reduces the vapor gradient and prevents transpiration rate from changing. Since E has not changed, the expression for E (Equation 1) can be set equal for nitox and helox, leading to a result in which h is the only unknown:

$$E' = E \;\rightarrow\; \frac{\eta(hw_s' - w_a')}{1 - \frac{1}{2}(hw_s' + w_a')} = \frac{hw_s - w_a}{1 - \frac{1}{2}(hw_s + w_a)}\,. \qquad (2)$$

In Equation 2, primes denote values in helox, and $\eta \equiv g_{tw}'/g_{tw}$ is the proportion by which helox increases g_{tw}. To a first approximation, $\eta \approx 2.33$, the ratio of the binary diffusivities for water vapor in helox and nitox. Equation 2 can be solved for h, given known values of w_s and w_s' (calculated from leaf temperature), and of w_a and w_a' (which are measured directly). Several other studies have also used helox to study leaf gas exchange, albeit for different purposes (Parkhurst & Mott, 1990; Mott & Parkhurst, 1991; Mott *et al.*, 1993; Shope *et al.*, 2008; Šantrůček *et al.*, 2014).

Equation 2 assumes that h does not change when nitrogen is replaced with helium. In the limit of small distances from the site of evaporation, vapor is in equilibrium with liquid water in the apoplast (Nobel,

2020), which implies that $h \approx \exp(\psi_{apo}/y)$, where ψ_{apo} is the apoplastic water potential and $y \equiv RT/V_w$ (R is the gas constant, T the absolute temperature, and V_w the molar volume of water). In turn, ψ_{apo} is determined by the total flow through liquid-phase pathways proximal to the evaporating sites, and by the resistance of those pathways. Therefore, if E does not change in helox, then neither should ψ_{apo}, nor h.

The objective of this paper is to develop this method further, both theoretically and experimentally, and to demonstrate its application in several species, including some hypostomatous species, which cannot be examined by the Wong method. In particular, we relax the assumption that $\eta = 2.33$ to account for different effects of helox on boundary layer and cuticular transport, and we explore how to interpret results in the context of a model in which large vapor gradients may occur within the leaf.

Methods

Theory

To apply Eqn 2 to real experimental data, it is necessary to account for the fact that E in helox (E') will never be quite exactly equal to E in nitox. Allowing for $E/E' = \varepsilon$, where ε is a number very close to 1 but determined experimentally as the ratio of measured E and E', Eqn 2 is modified to

$$E' = E \;\rightarrow\; \frac{\epsilon\eta(hw_s' - w_a')}{1 - \frac{1}{2}(hw_s' + w_a')} = \frac{hw_s - w_a}{1 - \frac{1}{2}(hw_s + w_a)}. \qquad (3)$$

(Methods S1 evaluates the potential effect of any bias caused by $\varepsilon \neq 0$, and finds it negligible.) Solving Equation 3 for h gives

$$[(\epsilon\eta - 1)w_s'w_s]h^2 + [2(w_s - \epsilon\eta w_s') + (\epsilon\eta + 1)(w_s'w_a - w_s w_a')]h + [2(\epsilon\eta w_a' - w_a) - (\epsilon\eta - 1)w_a w_a'] = 0, \qquad (4)$$

which is quadratic in h, so h can be computed as

$$h = \frac{1}{2a}\left[-b - \sqrt{b^2 - 4ac}\right], \qquad (5)$$

where

$$a = (\epsilon\eta - 1)w_s' w_s, \quad (5a)$$

$$b = 2(w_s - \epsilon\eta w_s') + (\epsilon\eta + 1)(w_s' w_a - w_s w_a'), \quad (5b)$$

$$c = 2(\epsilon\eta w_a' - w_a) - (\epsilon\eta - 1)w_a w_a'. \quad (5c)$$

To calculate *h* from Eqn 5, one requires values for w_s', w_s, w_a', w_a and η. The first four of these are either directly measured (w_a, w_a') or calculated from measured leaf temperature (w_s, w_s'). Estimation of η (discussed below) requires knowledge of the ratios of stomatal, cuticular and boundary layer conductance, yet to know stomatal conductance, one must know *h*; thus, in practice, estimation of *h* requires iterative numerical solution, despite the apparent analytical solution given by Eqn 5.

Estimating η

Helox increases the diffusivity of water vapor by a factor 2.33 (Egorov & Karpushkin, 1988), so to a first approximation, η = 2.33. However, there are two important caveats. First, this tacitly assumes that the only change in g_{tw} is that due directly to helox – i.e., stomatal apertures do not change. We suggest that this is a safe assumption, given that, by design, *E* does not change, and as shown by Mott and Parkhurst (1991) (also using helox), stomata sense something closely tied to *E*; other work in the intervening years has concluded that stomata sense the bulk symplastic water status of the leaf (Buckley, 2005, 2019), probably via some property closely tied to the volumes of mesophyll cells (McAdam & Brodribb, 2018; Sack *et al.*, 2018). Thus, if *E* is unchanged, it is likely the case that symplastic water status and hence stomatal aperture are also unchanged.

Second, η would not generally be exactly 2.33, because transport through the boundary layer (Monteith & Unsworth, 1990) and probably through the cuticle (Becker *et al.*, 1986) do not occur purely by gas-phase diffusion. g_{tw} is the sum of conductances at each surface:

$$g_{tw} = \frac{(g_{sw} + g_{cw})g_{bw}}{g_{sw} + g_{cw} + g_{bw}} + \frac{(sg_{sw} + g_{cw})g_{bw}}{sg_{sw} + g_{cw} + g_{bw}} \quad (6)$$

where g_{cw}, g_{sw} and g_{bw} are the abaxial cuticular, stomatal and boundary layer conductances to water vapor, respectively, and *s* is the ratio of stomatal conductances between the adaxial and abaxial surfaces. Equation 6 assumes neither cuticular nor boundary layer conductance differs between the two leaf surfaces. Rearrangement gives

$$g_{tw} = \frac{g_{sw}\left(1+\frac{g_{cw}}{g_{sw}}\right)}{\frac{g_{sw}}{g_{bw}}\left(1+\frac{g_{cw}}{g_{sw}}\right)+1} + \frac{g_{sw}\left(s+\frac{g_{cw}}{g_{sw}}\right)}{\frac{g_{sw}}{g_{bw}}\left(s+\frac{g_{cw}}{g_{sw}}\right)+1} = g_{sw}\left[\frac{1+\phi}{\gamma(1+\phi)+1} + \frac{s+\phi}{\gamma(s+\phi)+1}\right] \quad (7)$$

where $\phi \equiv g_{cw}/g_{sw}$ and $\gamma \equiv g_{sw}/g_{bw}$. Thus,

$$\eta \equiv \frac{g'_{tw}}{g_{tw}} = \frac{g'_{sw}}{g_{sw}} \cdot \frac{\left[\frac{1+\phi\left[\frac{\phi'}{\phi}\right]}{\gamma\left[\frac{\gamma'}{\gamma}\right]\left(1+\phi\left[\frac{\phi'}{\phi}\right]\right)+1} + \frac{s+\phi\left[\frac{\phi'}{\phi}\right]}{\gamma\left[\frac{\gamma'}{\gamma}\right]\left(s+\phi\left[\frac{\phi'}{\phi}\right]\right)+1}\right]}{\left[\frac{1+\phi}{\gamma(1+\phi)+1} + \frac{s+\phi}{\gamma(s+\phi)+1}\right]} \quad (8)$$

where primes denote values in helox. The ratio g_{sw}'/g_{sw} is 2.33, because transport through the stomatal pore is strictly diffusive. Calculating η also requires estimates of γ, ϕ, $[\gamma'/\gamma]$ and $[\phi'/\phi]$. Below we discuss the latter two ratios first, and then we describe how we estimated ϕ and γ themselves.

[γ'/γ]. In laminar flow, the Pohlhousen equation (Schuepp, 1993) predicts $g_{bw}'/g_{bw} = 2.33^{2/3} \approx 1.76$, reflecting the fact that laminar boundary layer transport is partly diffusive and partly advective. Under turbulent conditions, transport is entirely advective and g_{bw}'/g_{bw} should be close to unity (Monteith & Unsworth, 1990). Thus, g_{bw}'/g_{bw} should be between 1 and 1.76. In practice, we estimated g_{bw}'/g_{bw} experimentally by measuring the total conductance of a wet filter paper (a model of a leaf with zero stomatal and cuticular resistance) in nitox and helox, and found $g_{bw}'/g_{bw} = 1.58$; thus, in our experimental system, $\gamma'/\gamma = (g_{sw}'/g_{bw}')/(g_{sw}/g_{bw}) = (g_{sw}'/g_{sw})/(g_{bw}'/g_{bw}) = 2.33/1.58 = 1.47$.

[ϕ'/ϕ]. Although the transport mode for water movement across the cuticle is not known with certainty, we are not aware of any experimental evidence that it occurs by gas-phase diffusion. Becker et al. (1986) suggest cuticular transport occurs by diffusion in solution, through the solid matrix of the cuticle itself, which should be unaffected by helium. Thus, we assume $g_{cw}'/g_{cw} \approx 1$, giving $\phi'/\phi = (g_{cw}'/g_{sw}')/(g_{cw}/g_{sw}) = (g_{cw}'/g_{cw})/(g_{sw}'/g_{sw}) = 1/2.33 \approx 0.429$.

ϕ and γ. The ratios of g_{cw} to g_{sw}, and of g_{sw} to g_{bw}, cannot be known prospectively, because that would require knowledge of the true value of g_{sw}, which in turn depends on the unknown value of intercellular relative humidity. Thus, in practice, we estimated g_{sw} (and hence ϕ and γ) by iterative

numerical solution of Eqn 5 and 8 using function optimize() in R; this requires an initial estimate of g_{sw}, which we provided by calculating g_{tw} assuming h = 1 and then solving Eqn 6 for g_{sw}, given g_{cw} and g_{bw}. We estimated g_{cw} using values previously published in the literature for each species; these ranged from 0.00036 mol m^{-2} s^{-1} to 0.00427 mol m^{-2} s^{-1} (note, these are abaxial values; double them to obtain whole-leaf equivalent values) (Table S1).

"Back of the envelope" estimate of h ($\hat{h}$). To quantify the degree to which the estimate of h depends on factors such as ϕ, γ, and the terms other than unity in the denominator of Eqn 1 (which account for the interaction between air and water vapor), we also calculated h using a highly simplified expression, in which η is simply assumed to equal 2.33 (thus ignoring the complicating influences of boundary layer and cuticular transport) and $\overline{w}$ is ignored (ignoring the air-vapor interactions), which gives

$$\hat{h} = \frac{2.33w'_a - w_a}{2.33w'_s - w_s} \quad (9)$$

Two-point model of leaf interior

The preceding analysis treats the leaf interior as a single point, with one site of evaporation and, implicitly, no vapor gradient within the leaf. If large vapor gradients do occur within the leaf, then switching to helox would affect those gradients, complicating the interpretation of h. To address this, in Methods S2 we analyzed a two-point model of the leaf interior, in which water can evaporate either from a proximal site (deep within the leaf) or from a distal site (near the stomatal pore), and water vapor can diffuse from the proximal site to the distal site. Our analysis allows for a wide range of liquid-phase resistances from the xylem to the apoplastic water at each evaporating site, and also of the vapor-phase resistance between the two evaporating sites (Tables S2, S3). A key conclusion from that analysis is that the 'naive' approach based on a single-point model of the leaf interior (Eqn 5) would always overestimate the intercellular relative humidity at the distal evaporating site and underestimate its value at the proximal site. Thus, our naive estimates likely represent the true intercellular relative humidity somewhere within the leaf.

Gas exchange measurements

Gas exchange system

We measured gas exchange rates and controlled ambient conditions around the leaf using a custom open flow gas exchange system based on two Li-7000 differential infrared gas analyzers (LI-COR, Lincoln, NE). A diagram illustrating the flow of gases through the system and its major components is provided in Fig S1. The main carrier gas (N_2 or He) flowed from high-pressure tanks through two mass flow controllers (MFCs; FMA-5400 series, Omega, Norwalk, CT). Air from one of the MFCs was kept dry, while air from the other MFC was humidified by passing it through an aquarium aeration stone in a 2000-mL beaker containing degassed water to saturate it with water vapor, then through a Graham condenser (whose temperature was controlled by water flowing from a recirculating chiller) to reduce the dewpoint to a fixed value. We used separate humidifiers (beaker + condenser) for nitrogen and helium. The humidified and dry gas streams were then recombined. By adjusting the relative flow rates through the 'wet' and 'dry' MFCs, we could rapidly and precisely modulate the vapor content of the gas stream. Oxygen and CO_2 were injected into the recombined gas stream using MFCs (O_2: FMA-5400 series, Omega; CO_2: MC-2SCCM, Alicat Scientific, Tucson, AZ) to give 21% O_2 and, typically, about 450 μmol/mol CO_2. After passing through a length of tubing (~15 cm) containing debraided copper wire to promote uniform mixing, the airstream was then split equally into reference and sample streams.

The sample stream passed through a mass flow meter (MFM; FMA-2000 series, Omega) and then through a cuvette containing the leaf (the cuvette is described below); the reference stream passed through an identical flow meter and an identical but empty cuvette. Each stream then passed through a pair of rotameters (model 6AP2116M1, Dakota Instruments, Orangeburg, NY) to balance flows as described below, then through the sample cell of an IRGA, and finally through a chilled mirror dewpoint hygrometer (General Eastern DEW-10, GE Sensing, Billerica, MA). The reference cell of each IRGA contained dry and CO_2-free air recirculated through a scrubber (containing indicating silica gel and Ascarite II) using the IRGA's built-in pump. The difference in pressure between the two streams was monitored using a digital differential pressure sensor (model SSCSNBN001NDAA5, Honeywell, Richardson, TX) proximal to the rotameters, and kept below 20 Pa in magnitude.

To balance flows and enable matching (sending identical gas through the sample cell of both IRGAs), each flow stream (reference and sample) was split into two equal components before entering the rotameters; both streams passed through rotameters with fine needle valves, but only one of the two

streams (termed the "primary" stream) was sent to a gas analyzer at any given time, while the other (termed the "null" stream) was vented to the atmosphere. During matching, the reference null stream was swapped with the sample primary stream, such that the reference null stream passed through the sample IRGA and the sample primary stream passed through the reference null stream's rotameter. The same procedure could also be used to match the IRGAs using sample gas rather than reference gas. This design (illustrated in Fig S2) ensured that the total flow through each stream, and hence the flow through the leaf cuvette and the pressures in the IRGA cells, did not change during matching.

Calibration

Each IRGA was calibrated daily in nitox, using the chilled mirror dewpoint hygrometers as an absolute calibration reference for H_2O and pre-mixed calibration gas containing 395.2 ppm CO_2. The hygrometers are not suitable for primary measurements during the experiment because they respond too slowly to changes in gas composition; however, they were useful for calibration, provided adequate time was given to allow them to fully stabilize (we typically waited 10 min).

Additionally, before conducting any experiments, we calibrated each IRGA separately in nitox and helox to quantify how the IRGA's output differed between the two gases. We generated nitox or helox with 21% O_2 and 450 ppm CO_2 using MFCs as described earlier (the MFCs were calibrated volumetrically as described below), and adjusted the humidified proportion of total flow across a wide range to generate a range of humidities. At each humidity, we allowed 20-30 min for each analyzer and hygrometer to stabilize, then used the hygrometer reading as the true value of water vapor mole fraction and computed second-order polynomial expressions relating the apparent (uncorrected) IRGA readings in helox to the calibrated readings in nitox. The calibrations were nearly linear, but we fitted second-order polynomials for maximum accuracy (Fig S3); these calibrations corresponded to a correction factor of approximately 1.6 for water vapor in helox (i.e., the IRGA signal for water vapor concentration would need to be multiplied by approximately 1.6 in helox to obtain the true vapor concentration).

We used custom-built bubble flowmeters to calibrate the leaf cuvette MFM and MFCs; these calibrations were repeated in nitox and helox (for the cuvette MFM), in N_2 and He (for the wet and dry MFCs), or in O_2 (for the O_2 MFC). A given MFC or MFM was arranged in series with a vertically-oriented transparent cylinder marked with graduations indicating volume increments, and bubble-detector fluid (Better Bubble, RectorSeal, Houston, TX) was injected into the airstream in the bottom of the cylinder to

create fine bubble films that migrated up the cylinder as air flowed through the cylinder to the atmosphere. We measured flow rates by timing the movement of bubble films past given numbers of graduations, and used the resulting values of flow rate to generate calibration polynomials for each MFM or MFC. The MFCs that controlled flows of pure N_2 and He required a correction of approximately 1.458 for He (i.e., the uncalibrated helox flow rates reported by the device were about 1/1.458 = 68.6% of the true volumetric rates), which was similar to the nominal correction factor of 1.454 suggested in the MFC manual. For helox passing through the cuvette MFM, the correction factor was approximately 1.415. In practice, we used 2nd-order polynomials for each unit (Fig S4 shows the calibrations for the MFM).

Leaf cuvettes

Each cuvette (Figs S5 and S6) was milled from aluminum and nickel-plated to reduce water vapor adsorption; all interior surfaces were also sprayed with Teflon spray (Dupont, Wilmington, DE) to further reduce adsorption. The main portion of the cuvette interior, where a leaf could sit, was 4 cm x 12 cm; beyond one end of that portion was a 40 x 40 mm cavity containing a fan (model MF40201VX-1000U-A99, Sunon, La Verne, CA), and beyond the opposite end was an empty 40 x 20 mm cavity. These cavities connected the leaf volume with a set of channels and fins milled into the bottom of the cuvette body; below that was an aluminum plate affixed to the main body with screws and sealed with a gasket made from dental putty (Zhermack Elite HD+ Light body fast set, Zhermack SpA, Badia Polesine, Italy). The fan circulated air across the leaf and then through the fin channels, producing a total (2-sided) boundary layer conductance in nitox of 4.5 mol m^{-2} s^{-1} for a 20 cm^2 leaf (5 cm wide in the direction of fan circulation flow) (measured using wet filter paper as a model of a leaf with no stomatal resistance). Water from a recirculating chiller (model 1160S, VWR, Radnor, PA) flowed through several channels in the cuvette body to control leaf temperature; that water did not come into contact with the air in the cuvette.

The leaf sat on top of the main cuvette body and below a lid (milled from aluminum with a glass window) that was secured using latches (model 4438N11, McMaster-Carr, Elmhurst, IL). The lid, main body and leaf were sealed against leaks using custom gaskets 3 mm thick and 10 mm wide made from silicone (Ecoflex 00-30, Smooth-On, Inc., Macungie, PA) using a custom machined aluminum mold. Fishing lines affixed to the chamber and the lid with 3.17 mm-diameter PTFE pegs were used to keep the leaf stable. Leaf temperature was measured using a 44-gauge fine-wire Type E thermocouple (model

CHCO-002-24, Omega) appressed to the lower leaf surface. To prevent the fine thermocouple junction from collapsing under the force of contact with the leaf, we embedded the space below the junction and between the two wires with molten polyethylene. Light was provided by a white LED light source (model Zinqolay, FECiDA, Zhongshan, China) fixed above the chamber lid. PPFD at the leaf surface was calculated from the distance of the light source to the chamber lid, using a calibration obtained by placing a LI-COR quantum sensor (model Li-190R, LI-COR) beneath the chamber lid, at the typical position of the leaf, and placing the light source at various distances from the lid. PPFD at the leaf surface varied by less than 11% across the central region of the cuvette (Fig S7b). We also tested variation in leaf temperature with thermocouple position across a 40 x 40 mm region for a *Helianthus annuus* leaf illuminated at 900 μmol m^{-2} s^{-1} PPFD and transpiring at 4.2 mmol m^{-2} s^{-1}, and found a standard deviation of 0.08 °C and a maximum range of 0.27 °C (Fig S7a).

Interrogation and control

All devices were monitored and/or controlled using a datalogger (CR6, Campbell Scientific Inc., Logan, UT) and multiplexers (AM16-32A, Campbell Scientific) operated via a custom interface built using Campbell Scientific RTMC software. To supply an accurate reference temperature for thermocouple measurements, we measured the temperature at the datalogger inputs used for thermocouple measurement using a platinum-resistance temperature detector (model PR-25AP-1/10-600-1/4-M12, Omega). Chamber gas composition could be rapidly adjusted by changing the control voltages sent to the mass flow controllers that mixed the gases, and leaf temperature could also be controlled by adjusting the target temperature of the recirculating water bath.

Approach to overcoming mixing and desorption lag artefact

When gas composition is changed, gas with the new composition normally reaches the reference IRGA faster than it reaches the sample IRGA, because the sample gas has to pass through the sample cuvette volume first. As a result, reported gas exchange rates typically contain a transient artefact for a period of time after changing reference gas composition. Moreover, the nature of this effect is more than a mere delay, or 'lag', because the new gas has to replace all of the old gas in the sample cuvette. This problem is more severe for water vapor than for CO_2, because water vapor tends to adsorb on cuvette surfaces, even if they have been nickel-plated. To minimize this artefact, we made the reference and sample flow paths identical: both passed through identical MFMs and leaf cuvettes (the cuvette in the reference flow path contained no leaf), all tubing lengths and fittings were identical in each path, and rotameters and a

differential pressure sensor were used to ensure that flow rates and pressures were also identical in each path. Fig S8 shows the result of empty-chamber tests (timecourses of reported transpiration rate following a large change in water vapor composition of the reference gas stream) with and without an empty cuvette in the reference line. Without the reference cuvette, the calculated transpiration rate is artefactually large in magnitude (1.07 mmol m^{-2} s^{-1} at 60 seconds after the change in gas composition), whereas including the reference cuvette reduces the transient artefact by 99.4% (0.0063 mmol m^{-2} s^{-1}). These measurements used a chamber flow rate of 1.26 L min^{-1} (847 μmol s^{-1}), and the calculations assumed a leaf area of 20 cm^2, both of which were typical of most experiments reported below.

Experimental procedure

After calibration each morning, the leaf was brought to steady-state gas exchange under given conditions. Reference CO_2 mole fraction was set to 450 μmol mol^{-1}, leaf cuvette flow rate was set to 1-2 L min^{-1} (672 – 1344 μmol s^{-1}), PPFD at the leaf surface was set to 982 – 1097 μmol m^{-2} s^{-1}, and the temperature of the water flowing through the cuvette body and humidifier condensers was set to 24.2°C (to achieve a leaf temperature of approximately 25°C), which was typically below the ambient temperature in the laboratory. Although we could easily adjust the water vapor mole fraction in the sample stream, in the initial experiments presented here we typically set the initial reference flow in nitox to 100% dry air and allowed the sample value to settle at whatever value arose from the balance between transpiration (which adds water vapor, humidifying cuvette air) and flow rate (which adds dry air to the cuvette); if the resulting value was below the effective measuring range of the chilled mirror dewpoint hygrometers (about 4 mmol mol^{-1}), we decreased cuvette flow to increase cuvette vapor concentration. This particular choice is not essential to the method, but instead was chosen in early experiments in order to facilitate tests of the system. Future experiments will vary the vapor composition of the sample stream in nitox.

Once gas exchange was steady, we replaced nitrogen with helium by operating a set of manual switching valves (model HV-02, VIILOCK, Yueqing, China); simultaneously, we increased the 'wet' flow (the portion of helium flow that was humidified) and decreased the 'dry' (non-humidified) flow by equal amounts, in order to increase water vapor mole fraction in the cuvette to a given level, chosen to produce the same transpiration rate that had occurred in nitox. In practice, this often required a series of small adjustments in wet and dry flows. Once transpiration was stable again, helium was replaced with nitrogen and the reference gas composition was returned to 100% dry air. This cycle was repeated

at least two more times under any given conditions (three total switches). In general, each "switch" to helox was completed within five minutes, including 1-2 minutes to achieve steady gas exchange measurements and another 2-4 minutes to verify that transpiration rate and stomatal conductance were unchanged and steady relative to their values in nitox. We then applied the resulting successive steady-state values of gas exchange parameters in nitox and helox to Eqn 5 to calculate intercellular relative humidity.

Plant material

Individuals of *Gossypium hirsutum* L., *Helianthus annuus* L., *Heteromeles arbutifolia* M.Roem., *Laurus nobilis* L., *Liriodendron tulipifera* L., *Magnolia grandiflora* L., *Oryza sativa* L. ('Nipponbare'), and *Pyrrosia hastata* Ching were grown in a greenhouse facility in Davis, California, from spring to winter 2025-2026. *G. hirsutum*, *Heteromeles arbutifolia*, and *O. sativa* were grown from seed in 7.5 L pots of UC Agronomy mix soil and maintained with drip fertigation using UNI-Old solution, a modified Hoagland solution (150:50:200 ppm N:P:K). *O. sativa* ('Nipponbare') was selected as it is widely used for reverse genetics and has a fully sequenced genome. *G. hirsutum* and *Helianthus annuus* were included as proof of concept, having been previously studied by Wong et al. (2022). *Laurus nobilis*, *M. grandiflora*, *Heteromeles arbutifolia*, *Liriodendron tulipifera*, and *P. hastata* were selected to represent phylogenetic diversity and for their hypostomatous leaves, a leaf type that cannot be investigated with the Wong method. Woody species were pruned as needed for canopy maintenance but not within six weeks before measurements. All plants were watered to saturation daily to prevent water stress.

Individual potted plants were moved into the laboratory the day before measurements to allow for acclimation and placed in trays of deionized water to ensure adequate hydration. Plants were placed under full-spectrum lighting (PPFD = 800-1600 µmol m^{-2} s^{-1}) on a 700-1900 h photoperiod with dark conditions overnight. Only fully expanded, light-exposed adult leaves were selected for measurements. Plants that had begun flowering were excluded. For gas exchange measurements, an intact leaf (still attached to the plant) was enclosed in the cuvette and allowed to equilibrate under given conditions (Table 2) before conducting the helox switch procedure described earlier. Pots were kept in trays with water to ensure the soil remained hydrated during the experiment.

Results

With the system described above, we were able to rapidly change the carrier gas from nitox to helox while simultaneously increasing the water vapor mole fraction of air exposed to the leaf, with the result that transpiration rate remained nearly unchanged. Figure 1 shows a typical run, in which the carrier gas is switched back and forth repeatedly. After the first switch, the operator makes a fine adjustment to the relative flows of dry and humidified gas in helox to better balance transpiration rates in nitox and helox – manifesting as a slightly lower reference vapor concentration in helox during the second switch as compared to the first (Fig 1b) – after which E is equal in nitox and helox to within ± 0.6% (Fig 1a). The total conductance (Fig 1d) increases in helox, as predicted, but this is offset by an equal decline in the leaf-air vapor gradient (Δw, Fig 1e). Each switch takes about five minutes, including 1-2 minutes for vapor concentrations to stabilize, and 2-4 minutes to record stable E and g_{sw} to verify that they had not changed.

In most cases, E changed by less than 1.3% after switching to helox. We considered any switch in which E changed by more than 2.5% to be "failed" (6 of 120 switches), and excluded these from further analysis; of the remaining successful switches, the median absolute % change was 0.5%, and in 73% of switches, E changed by less than 1%. There was a slight bias towards increases in E in helox, but this did not result in any significant bias in inferred intercellular relative humidity (p = 0.52; Fig 2), consistent with our theoretical evaluation of the potential effect of this bias (Methods S1, Fig S9).

Inferred intercellular relative humidity (h) was well below saturation in all cases (Fig 3). The highest values were found for *Helianthus annuus* (94.2 ± 0.5%; mean ± SE) and the lowest for *Oryza sativa* (71.0 ± 2.4%) (Tables 2, 3). These corresponded to apoplastic water potentials at the evaporating site of -8.3 ± 0.8 MPa (*H. annuus*) and -47.8 ± 4.8 MPa (*O. sativa*). These results imply that, of the total humidity drawdown from saturation to ambient, the fraction that occurred in the vapor phase (i.e., the ratio of the true vapor gradient to that assuming saturation, $[w_i - w_a]/[w_s - w_a]$) ranged from a high of 89.4% (in *G. hirsutum*) to a low of 63.1% (in *O. sativa*) (Fig 4). There was no consistent relationship between intercellular humidity and either transpiration rate or Δw across species (Fig 5).

The estimate of h obtained by solving Eqns 5 and 8 by numerical iteration was closely and linearly related to the "rough estimate" given by Eqn 9, which ignores complicating factors such as boundary

layer, cuticular conductance, and binary interactions between water vapor and air (Fig 6). The best-fit line had a slope very close to unity and an intercept of about +0.7% ({h [Eqn 5]} = 1.007·{h [Eqn 9]} + 0.007; r^2_{adj} = 0.9943, $p < 2.2 \cdot 10^{-16}$), implying the rough estimate scales almost perfectly with the more rigorous calculation, but underestimates h by about 0.7% on average. The main factor causing slight divergence between the rigorous and rough estimates of h was the value of η, the proportion by which helox increased total vapor conductance (Eqn 8): as η decreased below the theoretical limiting value of 2.33 (which applies when all vapor transport occurs by diffusion), the error in the rough estimate of h increased. Thus, the rough estimate is most accurate under conditions in which η can be assumed to be very close to 2.33 – namely, when $g_{sw} \ll g_{bw}$ and $g_{sw} \gg g_{cw}$.

We also tested the effect of uncertainty in the value of cuticular conductance (g_{cw}), and found that, in most cases, overestimation of the true value of g_{cw} by 100%, or underestimation by 50%, would have caused less than a 2% error in the true value of h in most cases. Notable exceptions were in one leaf of *Liriodendron tulipifera* and in *M. grandiflora* measured in winter, in which errors were up to 3% and 4%, respectively (Fig 7), in both cases due very low stomatal conductances measured in those leaves (0.06 and 0.03 mol m^{-2} s^{-1}, respectively).

Simulations using two-point model of leaf interior

Our simulations comparing the one-point model of the leaf interior (on which our estimate of intercellular humidity using Eqn 5 is based) with a two-point model (Fig S10) that includes evaporating sites both deep in the leaf (proximal) and near the stomatal pore (distal) found that the helox-based inference of h should generally fall between the simulated values for the proximal and distal evaporating sites (h_p and h_d, respectively) (Fig S11, S12). Whether h was closer to h_p or h_d depended on the ratios among the resistances assumed in the two-point model, for liquid-phase transport from the xylem to each evaporating site, and for vapor-phase transport between the two sites. For example, if the model assumed that the liquid-phase resistances to each site were equal, then h was generally closer to h_d than to h_p; if instead it assumed that the resistance to the proximal site was much lower than that to the distal site (so that humidity at the proximal site remained close to saturation), then h depended more strongly on the magnitude of the vapor-phase resistance – being closer to h_p if vapor resistance were small, and closer to h_d if vapor resistance were large. Our simulations also predicted that helox would reduce any vapor gradient within the leaf (Fig S13), and that neither illumination-induced temperature

gradients within the leaf nor a systematic decrease in leaf temperature upon switching to helox should substantially affect our inferences (Figs S14, S15).

Discussion

Our refinement and application of the helox compensation method, originally devised by Egorov and Karpushkin (1988), for inferring the relative humidity of the intercellular airspaces (*h*) – in which the nitrogen in air is replaced with helium, thus accelerating vapor diffusion, but an increase in transpiration rate is prevented by also increasing ambient humidity – demonstrated that the EK method can be applied to diverse species, and validated previous reports (Cernusak *et al.*, 2018; Wong *et al.*, 2022; Jain *et al.*, 2025) that *h* can be substantially below 100%. As this helox-based approach represents a fourth independent experimental method demonstrating $h \ll 1$, our results solidify beyond reasonable question the reality of airspace unsaturation. Moreover, our results demonstrate substantial unsaturation even in unstressed leaves, because all of the measurements presented here were conducted on leaves at low to moderate evaporative demand, attached to potted plants in moist soil.

The helox compensation method has two strengths that have potential to make it more suitable to wide application than other methods. It is one of two methods – the other being that of Wong et al. (2022) – that can measure *h* using traditional gas exchange techniques, whereas the methods of Cernusak et al. (2018) and Jain et al. (2024) require additional specialized equipment (to measure online stable isotope discrimination orspectroscopically resolved fluorometry, respectively). The helox approach also has several advantages over the Wong method: (1) It can measure *h* in hypostomatous leaves; by contrast, the Wong method only works on broad amphistomatous leaves, which represent a small fraction of the world's flora. We thus conducted the first purely IRGA-based validation of unsaturation on hypostomatous species in the modern era (namely, on *Heteromeles arbutifolia*, *M. grandiflora, Laurus nobilis*, *Liriodendron tulipifera*, and *Pyrrosia hastata*). (2) Unlike the Wong method, the helox compensation method does not require reducing CO_2 assimilation rate to zero at one leaf surface by lowering ambient [CO_2] to the compensation point at that surface. Nulling assimilation at one surface represents an unusual condition, physiologically, and could have uncharacterized effects on the interaction among photosynthetic processes and stomatal control (Lawson, 2009; Lawson *et al.*, 2018), and possibly regulation of within-leaf water transport (Moshelion *et al.*, 2015). (3) It requires only a single differential gas analysis system, whereas the Wong method requires measuring gas exchange

independently at each surface. Given the high up-front cost of IRGAs, few labs have access to two complete gas exchange systems, so the helox method has the potential to expand access to experimental validation of unsaturation across species. Although we used two differential IRGAs with each operating in absolute mode (i.e., with reference gas of known composition circulating through each IRGA's reference cell), this is not required for the helox method, and in principle the approach could be applied with a single differential IRGA. (4) It does not inherently require measurement of CO_2 exchange, which both the Wong and Cernusak methods require (though for switches lasting longer than a few minutes, CO_2 measurements may be needed to measure, and if necessary to correct for, any changes in intercellular CO_2 concentration in helox that may induce a stomatal response; this is discussed further below). This has the advantage that, in principle at least, the method can be applied using much lower-cost sensors to measure water vapor concentration, such as the capacitive humidity sensors used in all currently available commercial porometers.

To be clear, whatever advantages the helox compensation method might have over other approaches, those advantages are not, at present, realistically accessible to most of the scientific community, given that it took considerable effort and experience to build the system that we used to implement the method. In order for the method to become more widely accessible, it would need to be engineered into a user-friendly commercial device. We failed in an earlier attempt to apply a related method using a commercial gas exchange system (Li-6800, Li-Cor), because the 6800's system for mixing gases and controlling flows and pressures relies on flow controllers and meters whose calibrations change in helox; the system's highly integrated design, which was designed to maximize user-friendliness for typical measurements in air, prevented us from isolating these components in order to recalibrate them in helox. We instead built a system that uses stand-alone IRGAs (Li-7000) and a handmade gas mixing and analysis system, which would be more difficult for other investigators to recreate than it would if the method could be directly applied using an Li-6800 (or similar system). However, calibration issues might be surmountable with cooperation with the manufacturer. Another limitation with commercial systems is that, to avoid contamination due to out-gassing of He from the humidifier column when switching to N_2 (or vice versa), the method requires separate humidifiers for helox and nitox. Overcoming this constraint with a commercial system would likely require placing custom humidifiers upstream of the system and bypassing its internal gas mixing controls. A more subtle challenge involves balancing the pressures in each IRGA cell in both helox and nitox: switching to helox changes the distribution of resistances within the system in ways that are difficult to predict, and this can lead to changes in the

distribution of flow between the reference and sample gas streams, and thus differences in pressure between the reference and sample IRGA cells. We overcame this problem by making the reference and sample streams physically identical, except for the presence of the leaf in the sample chamber. A collateral benefit of this design is that it essentially eliminates the transient artefact in calculated transpiration rate (and parameters derived from it, like stomatal conductance) that occurs after changing the reference gas composition (Fig S8). This approach would likewise be more difficult to implement using a stand-alone commercial system.

Irrespective of any potential advantages of one method over another, there is inherent advantage in the existence of multiple independent methods to quantify something so controversial and far-reaching as leaf airspace unsaturation. Indeed, as noted by Carl Sagan, "*Extraordinary claims require extraordinary evidence*" (Sagan, 2011). We, ourselves, did not have particularly high Bayesian credences about the validity of the unsaturation phenomenon until it had been demonstrated by multiple methods. To further validate and better understand the phenomenon, we suggest it would be tremendously advantageous to apply two or more of these methods in the same leaf, or at least in the same populations of leaves. Moreover, since each method is arguably best suited to identifying the intercellular relative humidity at a different location within the leaf – at cell surfaces within 20 μm of the viewed surface (Aquadust), just inside the stomatal pore (Wong), at the sites of carbonic anhydrase activity (Cernusak), or at the internal origins of vapor-phase diffusion pathways (helox) – combining the methods could also provide insights regarding the spatial distribution of unsaturation within in the leaf.

Leaf airspace unsaturation and its implications

Our data demonstrate substantial unsaturation in the leaf airspaces of six species, with species-level means as low as 71% (for *Oryza sativa*). Two of the species we examined – *Helianthus annuus* (sunflower) and *Gossypium hirsutum* (cotton) – were previously examined by Wong et al. (2022). For cotton, at a similar Δw, we found similar h as Wong et al. (94%), whereas for sunflower, we found higher h (90% at a Δw = 11 mmol mol^{-1} [this study], vs 83% at Δw = 12 mmol mol^{-1} [Wong]); however, h varied across sunflower leaves, with 3 of 16 leaves having h below 89%. Egorov and Karpushkin (1988) reported a similar range of intercellular relative humidities (from 83.4% to 99%), albeit in different species. These relative humidities imply that liquid water in the apoplast of evaporating sites is exceedingly low – averaging between -8.3 and -48 MPa across species (for *H. annuus* and *O. sativa*, respectively) – and far below published turgor-loss points for any of the species we measured (-1.09 to -2.53 MPa; Table 3).

570 Our data thus corroborate other recent reports, using other techniques, that concluded apoplastic water
571 potential at the evaporating site can be well below the turgor-loss point of adjacent living cells
572 (Cernusak *et al.*, 2018; Wong *et al.*, 2022; Jain *et al.*, 2025). We also report airspace unsaturation in a
573 fern (*Pyrrosia hastata*) for the first time. Together, these results imply the occurrence of very large
574 water potential gradients between the symplast and evaporating site of cells somewhere in the leaf,
575 which – combined with the co-occurrence of substantial transpiration – implies very large resistance for
576 water transport between the symplast and evaporating sites (Buckley & Sack, 2019). The properties of
577 that resistance and its biophysical origin are beyond the scope of the present study, and have been
578 discussed elsewhere (Rockwell *et al.*, 2022; Cernusak *et al.*, 2024; Jain *et al.*, 2025); we merely note that
579 the method presented here has potential to greatly facilitate the study of those properties, by making it
580 easier to quantify airspace unsaturation.
581
582 Our modeling analysis suggests that the estimates of *h* produced by current method, which, like all
583 traditional gas exchange measurements, treats the leaf interior as having a single evaporating site,
584 should represent the true value of relative humidity somewhere within the leaf airspaces, in most
585 conditions. Whether our estimate corresponds more closely to the relative humidity near evaporating
586 sites deep within the leaf or close to the stomatal pore depends on the relative resistances for liquid
587 water movement between the xylem and those evaporating sites, and for vapor transport between the
588 evaporating sites. The only scenario where our *h* estimate would not correspond to any location within
589 the leaf is when a large temperature gradient occurs within the leaf (for example, due to light
590 absorption by palisade near the adaxial surface) and the actual intercellular humidity is very close to
591 saturation (Fig S13). The error in that scenario is caused by divergence of the true intercellular
592 saturation vapor pressure from the experimental estimate, which is typically based on the temperature
593 of a thermocouple appressed to the abaxial surface; the possibility of such divergence, and its effect on
594 gas exchange calculations, has been noted previously (Mott & Peak, 2010; Buckley *et al.*, 2017) and is
595 not unique to the method presented here. We note that the Aquadust method has provided direct
596 evidence of gradients in water potential within the apoplastic space (Jain *et al.*, 2025), albeit within the
597 first 20 μm beneath the outer surface of the leaf. Those authors also introduced a continuum model of
598 parallel, coupled transport through the liquid and vapor paths within the leaf; our model can be
599 considered a limiting case of theirs, with two nodes at which water can change phases (one deep in the
600 leaf and another near the stomatal pore) rather than a continuum of such sites. Their simulations (their
601 Figure 4) suggested fairly small gradients of *h* within most of the extent of the leaf airspaces – varying by

602 less than 1% across 100 μm of intercellular airspace in maize – consistent with small values of ρ_V (the
603 ratio of vapor- to liquid-phase resistances) from our simulations and suggesting the value of *h* inferred
604 from our method may be a reasonable approximation for much of the leaf airspaces.
605
606 We did not attempt to control for increases in intercellular CO_2 concentration (c_i) that might occur due
607 to faster gas diffusion in helox; such changes could, in theory, induce a decline in stomatal aperture,
608 violating the assumptions of the method. Any such change in aperture would not occur instantaneously,
609 but instead would occur gradually over many minutes, yet we saw no evidence of systematic changes in
610 conductance over the ~5 minutes that each leaf spent in helox after each nitox-helox switch (e.g., Fig 1).
611 Nevertheless, future applications of the method could aim to simultaneously decrease ambient CO_2,
612 along with increasing ambient humidity, when switching to helox, to reduce the impact of any stomatal
613 response to c_i.
614

615 ## Conclusion

616 We further developed and applied the helox compensation method of Egorov and Karpushkin (1988), in
617 which helium is used to separate the effects of vapor gradient and diffusional conductance on vapor
618 flux, enabling inference of intercellular relative humidity. Our results confirm substantial unsaturation of
619 the airspaces in leaves, extending that finding to six species not previously measured (*Heteromeles*
620 *arbutifolia, Laurus nobilis, Liriodendron tulipifera, Magnolia grandiflora*, *Oryza sativa*, and *Pyrrosia*
621 *hastata*), and for the first time to a seedless plant (the fern *P. hastata*). This method can be applied to
622 any leaf under any nearly environmental conditions with a single infrared gas analysis system, thus
623 potentially expanding the capacity to quantify unsaturation beyond specialist labs.
624
625

Acknowledgements

TNB acknowledges support from the National Science Foundation (IOS Award #2307341) and the National Institute of Food and Agriculture (Hatch grant #CA-D-PLS-2790-H). ARJ acknowledges support from the National Science Foundation (Postdoctoral Research Fellowship in Biology, Award #2410582). We acknowledge helpful reviews from three anonymous referees on an earlier draft of this work, feedback and assistance with plant maintenance from Colleen Mills, Troy A. Williams, Theresa M. Rackson, Roslynd C. Hagino, David U. Smedley, and Yongtao Guan, and the gracious loan of a LI-7000 from Matthew E. Gilbert.

Author contributions

TNB built the experimental apparatus. ARJ and TNB conducted measurements and analysis and co-wrote and edited the manuscript.

Data availability

Data and code are available in a public GitHub repository at https://doi.org/10.5281/zenodo.22167504.

Competing interests

None declared.

References

Ackerson RC, Hebert RR. **1981**. Osmoregulation in cotton in response to water stress: I. Alterations in photosynthesis, leaf conductance, translocation, and ultrastructure. *Plant physiology* **67**: 484–488.

Becker M, Kerstiens G, Schönherr J. **1986**. Water permeability of plant cuticles: permeance, diffusion and partition coefficients. *Trees* **1**: 54–60.

Buckley TN. **2005**. The control of stomata by water balance (Tansley Review). *New Phytologist* **168**: 275–292.

Buckley TN. **2019**. How do stomata respond to water status? *New Phytologist* **224**: 21–36.

Buckley TN, John GP, Scoffoni C, Sack L. **2017**. The sites of evaporation within leaves. *Plant Physiology* **173**: 1763–1782.

Buckley TN, Sack L. **2019**. The humidity inside leaves and why you should care: Implications of unsaturation of leaf intercellular airspaces. *American journal of botany* **106**: 618.

Caemmerer S, Farquhar GD. **1981**. Some relationships between the biochemistry of photosynthesis and the gas exchange of leaves. *Planta* **153**: 376–387.

Cernusak LA, Ubierna N, Jenkins MW, Garrity SR, Rahn T, Powers HH, Hanson DT, Sevanto S, Wong SC, McDowell NG. **2018**. Unsaturation of vapour pressure inside leaves of two conifer species. *Scientific Reports* **8**: 7667.

Cernusak LA, Wong SC, Stuart-Williams H, Márquez DA, Pontarin N, Farquhar GD. **2024**. Unsaturation in the air spaces of leaves and its implications. *Plant, Cell & Environment* **47**: 3685–3698.

Egorov V, Karpushkin L. **1988**. Determination of air humidity over evaporating surface inside a leaf by a compensation method.

Farquhar GD, Raschke K. **1978**. On the Resistance to Transpiration of the Sites of Evaporation within the Leaf. *Plant Physiology* **61**: 1000–1005.

Gaastra P. **1959**. Photosynthesis of crop plants as influenced by light, carbon dioxide, temperature and stomatal diffusion resistance. *Meded Landbouwhogesch Wageningen* **59**: 1–68.

Henson I. **1982**. Abscisic acid and water relations of rice (Oryza sativa L.): sequential responses to water stress in the leaf. *Annals of Botany* **50**: 9–24.

Hussain SB, Stinziano J, Pierre MO, Vincent C. **2024**. Accurate photosynthetic parameter estimation at low stomatal conductance: effects of cuticular conductance and instrumental noise. *Photosynthesis research* **160**: 111–124.

Jain P, Huber AE, Rockwell FE, Sen S, Holbrook NM, Stroock AD. **2024**. New approaches to dissect leaf hydraulics reveal large gradients in living tissues of tomato leaves. *New Phytologist* **242**: 453–465.

Jain P, Liu W, Zhu S, Chang CY-Y, Melkonian J, Rockwell FE, Pauli D, Sun Y, Zipfel WR, Holbrook NM. **2021**. A minimally disruptive method for measuring water potential in planta using hydrogel nanoreporters. *Proceedings of the National Academy of Sciences* **118**: e2008276118.

Jain P, Sen S, Rockwell FE, Twohey III RJ, Huber AE, Desai SA, Wu I-F, De Swaef T, Ilman MM, Studer AJ. **2025**. Loss of conductance between mesophyll symplasm and intercellular air spaces explains nonstomatal control of transpiration. *Proceedings of the National Academy of Sciences* **122**: e2504862122.

Lawson T. **2009**. Guard cell photosynthesis and stomatal function. *New Phytologist* **181**: 13–34.

Lawson T, Terashima I, Fujita T, Wang Y. **2018**. Coordination between photosynthesis and stomatal behavior. In: W.W. Adams III IT, ed. Advances in Photosynthesis and Respiration. The leaf: A platform for performing photosynthesis. Cham, Switzerland: Springer, 141–162.

McAdam S, Brodribb T. **2018**. Mesophyll cells are the main site of abscisic acid biosynthesis in water-stressed leaves. *Plant Physiology* **177**: 911–917.

Monteith JL, Unsworth MH. **1990**. *Principles of Environmental Physics*. Oxford: Butterworth-Heinemann.

Moshelion M, Halperin O, Wallach R, Oren R, Way DA. **2015**. Role of aquaporins in determining transpiration and photosynthesis in water-stressed plants: crop water-use efficiency, growth and yield. *Plant, Cell & Environment* **38**: 1785–1793.

Mott K, Cardon Z, Berry J. **1993**. Asymmetric patchy stomatal closure for the two surfaces of Xanthium strumarium L. leaves at low humidity. *Plant, Cell & Environment* **16**: 25–34.

Mott KA, Parkhurst DF. **1991**. Stomatal responses to humidity in air and helox. *Plant, Cell and Environment* **14**: 509–515.

Mott KA, Peak D. **2010**. Stomatal responses to humidity and temperature in darkness. *Plant, Cell & Environment* **33**: 1084–1090.

Nobel PS. **2020**. *Physicochemical & environmental plant physiology, 5th edition*. Academic Press, Cambridge, Massachusetts.

Parkhurst DF, Mott KA. **1990**. Intercellular diffusion limits to CO2 uptake in leaves: studies in air and helox. *Plant physiology* **94**: 1024–1032.

Rockwell FE, Holbrook NM, Jain P, Huber AE, Sen S, Stroock AD. **2022**. Extreme undersaturation in the intercellular airspace of leaves: a failure of Gaastra or Ohm? *Annals of Botany* **130**: 301–316.

Sack L, John GP, Buckley TN. **2018**. ABA Accumulation in Dehydrating Leaves Is Associated with Decline in Cell Volume, Not Turgor Pressure. *Plant physiology* **176**: 489–495.

Sagan C. **2011**. *Broca's brain: Reflections on the romance of science*. Ballantine Books.

Salleo S, Nardini A, Pitt F, Gullo MAL. **2000**. Xylem cavitation and hydraulic control of stomatal conductance in laurel (Laurus nobilis L.). *Plant, Cell & Environment* **23**: 71–79.

Šantrůček J, Vráblová M, Šimková M, Hronková M, Drtinová M, Květoň J, Vrábl D, Kubásek J, Macková J, Wiesnerová D. **2014**. Stomatal and pavement cell density linked to leaf internal CO2 concentration. *Annals of Botany* **114**: 191–202.

Schuepp P. **1993**. Tansley review No. 59. Leaf boundary layers. *New Phytologist*: 477–507.

Scoffoni C, Vuong C, Diep S, Cochard H, Sack L. **2014**. Leaf shrinkage with dehydration: coordination with hydraulic vulnerability and drought tolerance. *Plant Physiology* **164**: 1772–1788.

Shope JC, Peak D, Mott KA. **2008**. Stomatal responses to humidity in isolated epidermes. *Plant, Cell & Environment* **31**: 1290–1298.

Wong SC, Canny MJ, Holloway-Phillips M, Stuart-Williams H, Cernusak LA, Márquez DA, Farquhar GD. **2022**. Humidity gradients in the air spaces of leaves. *Nature Plants* **8**: 971–978.

Supporting information

Tables

Table 1. List of mathematical parameters used in the main text, with symbols and units.

parameter	symbol	units
net CO_2 assimilation rate	A	μmol m^{-2} s^{-1}
2nd-order quadratic coefficient in solution for h	a	unitless
1st-order quadratic coefficient in solution for h	b	unitless
0th-order quadratic coefficient in solution for h	c	unitless
ambient CO_2 mole fraction	c_a	μmol mol^{-1}
intercellular CO_2 mole fraction	c_i	μmol mol^{-1}
^{18}O discrimination	$\delta^{18}O$	per mille
leaf to air water vapor mole fraction difference	Δw	mol mol^{-1}
transpiration rate in nitox	E	mol m^{-2} s^{-1}
transpiration rate in helox	E'	mol m^{-2} s^{-1}
ratio of transpiration rate in helox to nitox	ε	unitless
ratio of g_{cw} to g_{sw} in nitox	ϕ	unitless
ratio of g_{cw} to g_{sw} in helox	ϕ'	unitless
abaxial leaf boundary layer conductance to water vapor	g_{bw}	mol m^{-2} s^{-1}
abaxial leaf cuticular conductance to water vapor	g_{cw}	mol m^{-2} s^{-1}
abaxial stomatal conductance to water vapor	g_{sw}	mol m^{-2} s^{-1}
leaf total conductance to water vapor	g_{tw}	mol m^{-2} s^{-1}
ratio of g_{sw} to g_{bw} in nitox	γ	unitless
ratio of g_{sw} to g_{bw} in helox	γ'	unitless
intercellular relative humidity	h	unitless
rough estimate of h	$\hat{h}$	unitless
h at distal evaporating site in 2-point leaf model	h_d	unitless
h at proximal evaporating site in 2-point leaf model	h_p	unitless
ratio of g_{tw} in helox to nitox	η	unitless
gas constant	R	Pa m^3 mol^{-1} K^{-1}
ratio of adaxial to abaxial stomatal conductance	s	unitless
temperature	T	K
molar volume of water	V_w	m^3 mol^{-1}
ambient water vapor mole fraction in nitox	w_a	mol mol^{-1}
ambient water vapor mole fraction in helox	w_a'	mol mol^{-1}
intercellular water vapor mole fraction	w_i	mol mol^{-1}
saturated water vapor mole fraction in nitox	w_s	mol mol^{-1}
saturated water vapor mole fraction in helox	w_s'	mol mol^{-1}
composite parameter (RT/V_w)	y	MPa
water potential of apoplastic water	ψ_{apo}	MPa

Table 2. List of individual experiments, with mean ± SE (among technical replicates) of transpiration rate (E, mmol m^{-2} s^{-1}), leaf temperature (T, °C), ambient water vapor mole fraction (w_a, mmol mol^{-1}), leaf-to-air water vapor difference [corrected for unsaturation] (Δw, mmol mol^{-1}), and intercellular relative humidity (h, %). Each row is one leaf measured on a given day; n is the number of technical replicates per leaf (SE is omitted when n=1). GOHI: *Gossypium hirsutum*; HEAN: *Helianthus annuus*; HEAR: *Heteromeles arbutifolia*; LANO: *Laurus nobilis*; LITU: *Liriodendron tulipifera*; MAGR: *Magnolia grandiflora* [sp: spring (May 2025); wi: winter (January 2026)]; ORSA: *Oryza sativa*; PYHA: *Pyrrosia hastata*.

species	date	E	T	w_a	Δw	h	n
GOHI	2026-01-08	3.6	25.29	12.1	17.62	92.4	1
	2026-01-13	6.4 ± 0.0	25.02 ± 0.00	14.4 ± 0.0	15.33 ± 0.06	93.7 ± 0.3	2
	2026-01-14	4.8 ± 0.0	25.11 ± 0.01	14.5 ± 0.0	15.82 ± 0.01	95.1 ± 0.1	2
HEAN	2025-05-12	7.0 ± 0.0	23.46 ± 0.02	21.2 ± 0.0	5.47 ± 0.02	92.3 ± 0.1	4
	2026-01-07	7.9 ± 0.1	24.33 ± 0.01	19.9 ± 0.1	9.21 ± 0.10	95.5 ± 0.1	6
	2026-01-15	8.0 ± 0.0	24.29 ± 0.01	14.7 ± 0.1	13.40 ± 0.26	92.7 ± 0.8	3
	2026-02-09	6.6 ± 0.0	24.64 ± 0.01	20.0 ± 0.1	10.43 ± 0.10	98.1 ± 0.1	7
	2026-03-06	7.9 ± 0.1	24.74 ± 0.12	21.0 ± 0.2	9.59 ± 0.01	98.0 ± 0.0	2
	2026-03-11	6.2 ± 0.2	24.51 ± 0.10	18.4 ± 0.6	8.89 ± 0.77	88.7 ± 1.2	2
	2026-03-12	8.3 ± 0.0	24.45 ± 0.11	22.1 ± 0.1	7.98 ± 0.24	98.2 ± 0.2	2
	2026-03-13	8.7 ± 0.0	24.60 ± 0.00	22.9 ± 0.2	7.56 ± 0.21	98.5 ± 0.0	2
	2026-03-19	8.9 ± 0.0	24.33 ± 0.00	21.4 ± 0.2	8.60 ± 0.24	98.6 ± 0.3	2
	2026-03-23	7.5 ± 0.0	24.06 ± 0.03	22.9 ± 0.1	6.64 ± 0.10	98.6 ± 0.0	2
	2026-06-04	6.5 ± 0.2	24.62 ± 0.02	17.6 ± 0.4	11.65 ± 0.31	94.5 ± 0.5	5
	2026-06-08	6.1 ± 0.1	24.73 ± 0.01	13.9 ± 0.2	13.78 ± 0.11	88.9 ± 0.3	4
	2026-06-09	9.2 ± 0.0	24.24 ± 0.01	21.2 ± 0.1	8.45 ± 0.08	98.1 ± 0.1	4
	2026-07-13	4.7 ± 0.0	24.58 ± 0.01	13.7 ± 0.2	13.72 ± 0.67	88.7 ± 1.4	2
	2026-07-14	10.0 ± 0.1	24.56 ± 0.02	18.5 ± 0.1	9.93 ± 0.07	92.0 ± 0.1	3
	2026-07-15	6.2 ± 0.0	24.55 ± 0.02	16.7 ± 0.1	11.04 ± 0.11	90.0 ± 0.2	3
HEAR	2025-05-20	2.8 ± 0.0	22.09 ± 0.01	12.9 ± 0.1	11.43 ± 0.15	91.7 ± 0.3	3
	2025-05-21	3.2	25.35	11.1	16.30	84.6	1
LANO	2026-02-02	2.4	25.41	5.0	23.32	87.2	1
	2026-02-03	2.3 ± 0.0	25.33 ± 0.02	7.1 ± 0.1	21.02 ± 0.18	87.0 ± 0.5	2
	2026-02-04	2.1 ± 0.0	25.05 ± 0.00	7.3 ± 0.0	20.42 ± 0.06	87.3 ± 0.1	4
LITU	2026-06-10	2.7 ± 0.1	25.38 ± 0.02	7.7 ± 0.2	20.03 ± 0.38	85.6 ± 0.4	2
	2026-06-16	1.2	25.64	4.8	19.36	73.6	1
	2026-06-17	3.7 ± 0.3	25.06 ± 0.00	11.8 ± 0.9	16.03 ± 0.25	88.5 ± 2.0	2
	2026-06-23	3.2 ± 0.0	25.08 ± 0.00	7.9 ± 0.1	18.96 ± 0.09	84.5 ± 0.2	2
	2026-06-24	3.1 ± 0.0	25.12 ± 0.02	9.0 ± 0.1	18.43 ± 0.28	85.8 ± 0.7	3
	2026-06-30	2.8 ± 0.1	24.86 ± 0.03	9.0 ± 0.1	16.51 ± 0.80	81.1 ± 2.1	2
	2026-07-01	2.2 ± 0.1	25.33 ± 0.03	6.4 ± 0.1	19.84 ± 0.97	81.1 ± 2.8	2
	2026-07-08	3.6 ± 0.0	24.59 ± 0.01	13.7 ± 0.1	14.03 ± 0.25	89.8 ± 0.5	3
MAGR (sp)	2025-05-07	3.0 ± 0.0	25.32 ± 0.03	7.4 ± 0.0	15.87 ± 0.14	72.1 ± 0.4	4
MAGR (wi)	2026-01-27	1.5 ± 0.0	25.74 ± 0.01	4.6 ± 0.1	24.21 ± 0.16	87.2 ± 0.2	5
ORSA	2026-01-21	4.3 ± 0.1	25.27 ± 0.02	7.0 ± 0.2	15.94 ± 1.05	71.1 ± 3.8	4
	2026-01-22	4.3 ± 0.1	25.27 ± 0.02	7.0 ± 0.2	15.86 ± 0.98	70.9 ± 3.6	4
PYHA	2026-07-02	1.3 ± 0.0	24.80 ± 0.02	5.5 ± 0.1	16.89 ± 0.16	71.7 ± 0.8	3
	2026-07-06	2.5	25.13	7.7	19.66	85.6	1
	2026-07-07	1.8 ± 0.1	24.77 ± 0.01	5.5 ± 0.2	17.8 ± 0.07	74.6 ± 0.4	3

Table 3. List of species measured in this study, with mean transpiration rate (E, mmol m^{-2} s^{-1}), whole-leaf stomatal conductance (g_{sw}, mol m^{-2} s^{-1}, corrected for intercellular airspace unsaturation), estimated intercellular relative humidity (h, %) and water potential of apoplastic water at the evaporating site (ψ_{apo}, MPa), turgor loss points (TLP, MPa) from the literature, and number of biological replicates (different leaves) measured ("reps").

species	family	E	g_{sw}	h	ψ_{apo}	TLP	reps
Gossypium hirsutum L.	Malvaceae	5.2 ± 0.5	0.17 ± 0.02	94.0 ± 0.5	-8.5 ± 0.8	-2.40 (1)	3
Helianthus annuus L.	Asteraceae	7.4 ± 0.18	0.48 ± 0.03	94.2 ± 0.5	-8.3 ± 0.8	-1.09 (2)	16
Heteromeles arbutifolia M.Roem.	Rosaceae	2.9 ± 0.1	0.25 ± 0.02	90.0 ± 1.8	-14.7 ± 2.8	-2.53 (2)	2
Laurus nobilis L.	Lauraceae	2.2 ± 0.1	0.11 ± 0.002	87.2 ± 0.1	-18.8 ± 0.2	-2.26 (3)	3
Liriodendron tulipifera L.	Magnoliaceae	3.0 ± 0.2	0.18 ± 0.02	84.1 ± 2.4	-24.0 ± 2.0	-1.25 (4)	8
Magnolia grandiflora L.	Magnoliaceae	1.5 ± 0.0*	0.06 ± 0.00	87.2 ± 0.2	-19.0 ± 0.3	-2.06 (2)	1
		3.0 ± 0.0**	0.20 ± 0.03	72.1 ± 0.4	-45.1 ± 0.7		1
Oryza sativa L.	Poaceae	4.3 ± 0.0	0.14 ± 0.06	71.0 ± 2.4	-47.8 ± 4.8	-2.29 (5)	2
Pyrrosia hastata Ching	Polypodiaceae	1.7 ± 0.2	0.093 ± 0.007	75.6 ± 1.9	-38.8 ± 3.2	NA	3

*Measured in winter [01-2026] or **spring [05-2025]. Sources: (1) Ackerson and Herbert (1981), (2) Scoffoni et al. (2014), (3) Salleo et al. (2000), (4) Burlett et al. (2025) , (5) Henson (1982).

Figures

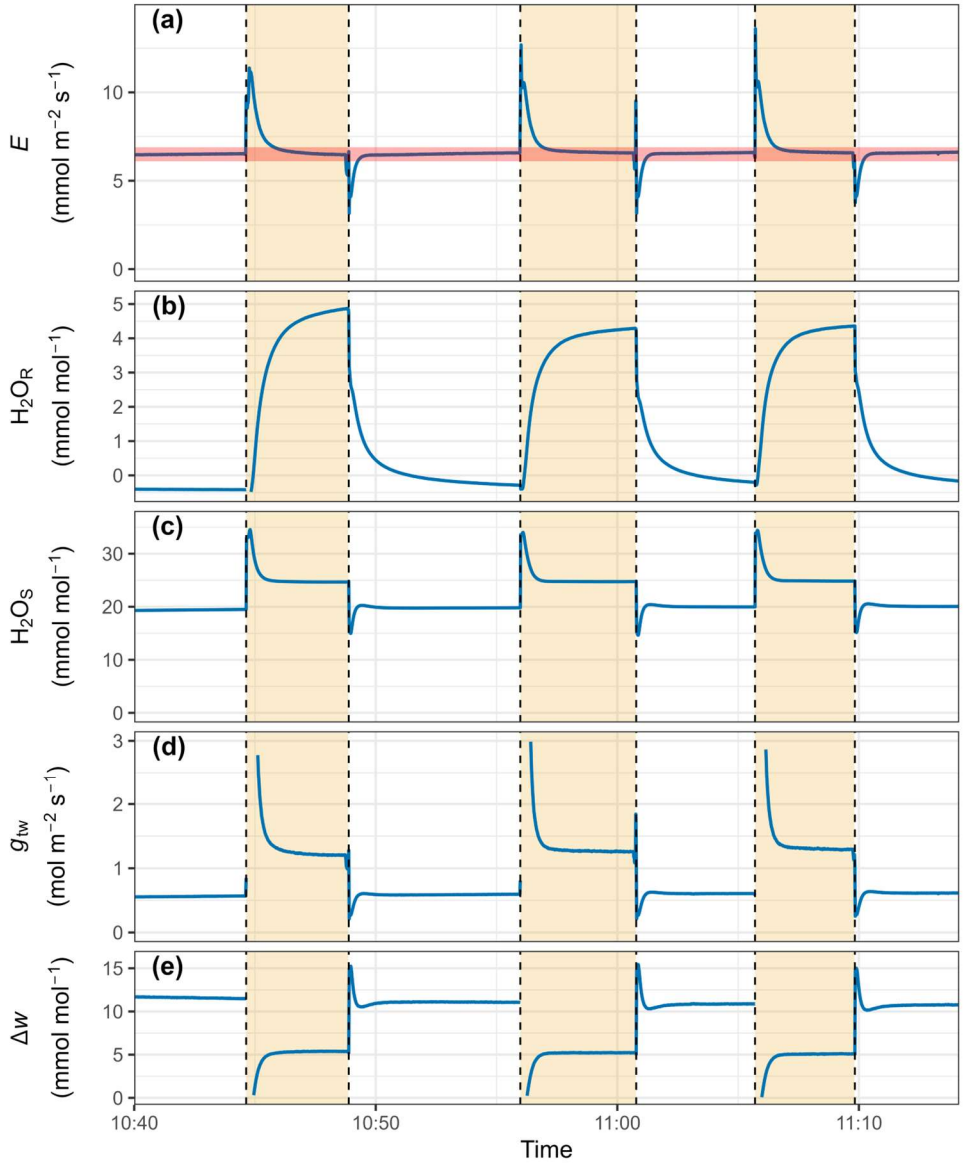

Figure 1. Illustration of changes in gas exchange parameters during a series of successive changes of the carrier gas back and forth between nitox (unshaded regions) and nitox (yellow-shaded regions), in a leaf of *Helianthus annuus*. Calculated transpiration rate (*E*, a) transiently increases upon each switch to helox, because changes in reference gas composition (H_2O_R, b) cause a transient condition of non-steady-state of sample gas composition (H_2O_S, c), but transpiration quickly stabilizes, along with calculated total conductance to water vapor (g_{tw}, d) and leaf-to-air water vapor mole fraction difference (Δw, e; the equivalent vapor pressure gradient [VPD_{leaf}] in kPa is $\Delta w/10$). After the first switch to helox, the operator makes a small adjustment in the target flowrate for humidified air, and thus for reference vapor composition, to better balance the transpiration rates in helox and nitox, after which steady-state transpiration rate is virtually identical in helox and nitox during successive switches.

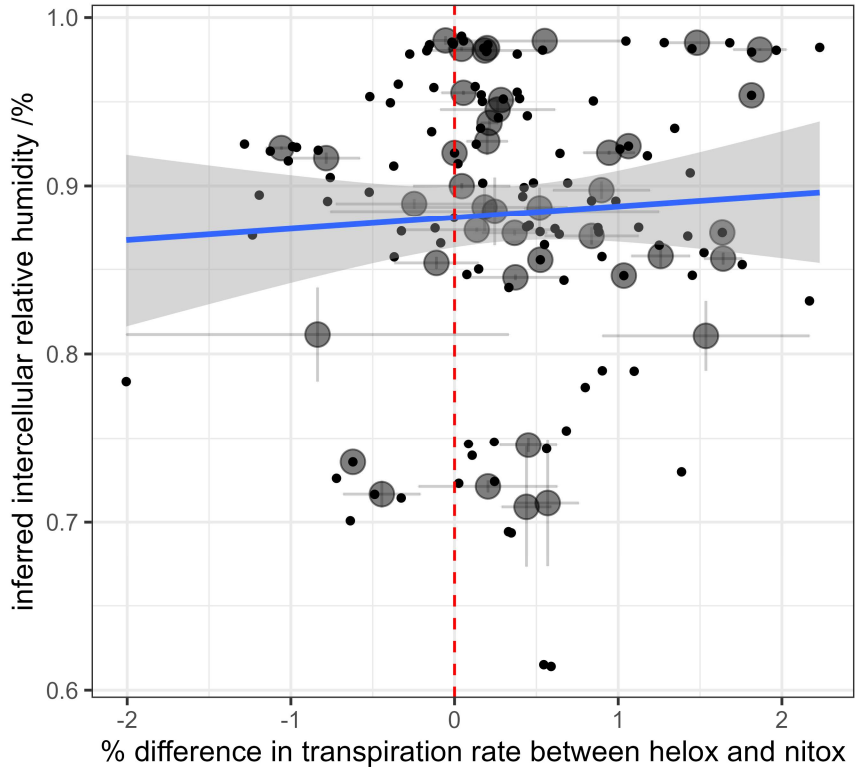

Figure 2. Inferred intercellular relative humidity was uncorrelated with the percent change in transpiration rate upon switching to helox. Blue line and shaded area = best fit linear regression ± 95% confidence intervals (n.s.; p = 0.516, r^2_{adj} = -0.0057); dashed red line = reference for zero % change in transpiration rate. Each small closed symbol represents one technical replicate (a measurement of intercellular relative humidity from one change from nitox to helox in a given leaf); large, semi-transparent symbols with error bars are means ± SEs across technical replicates for individual leaves.

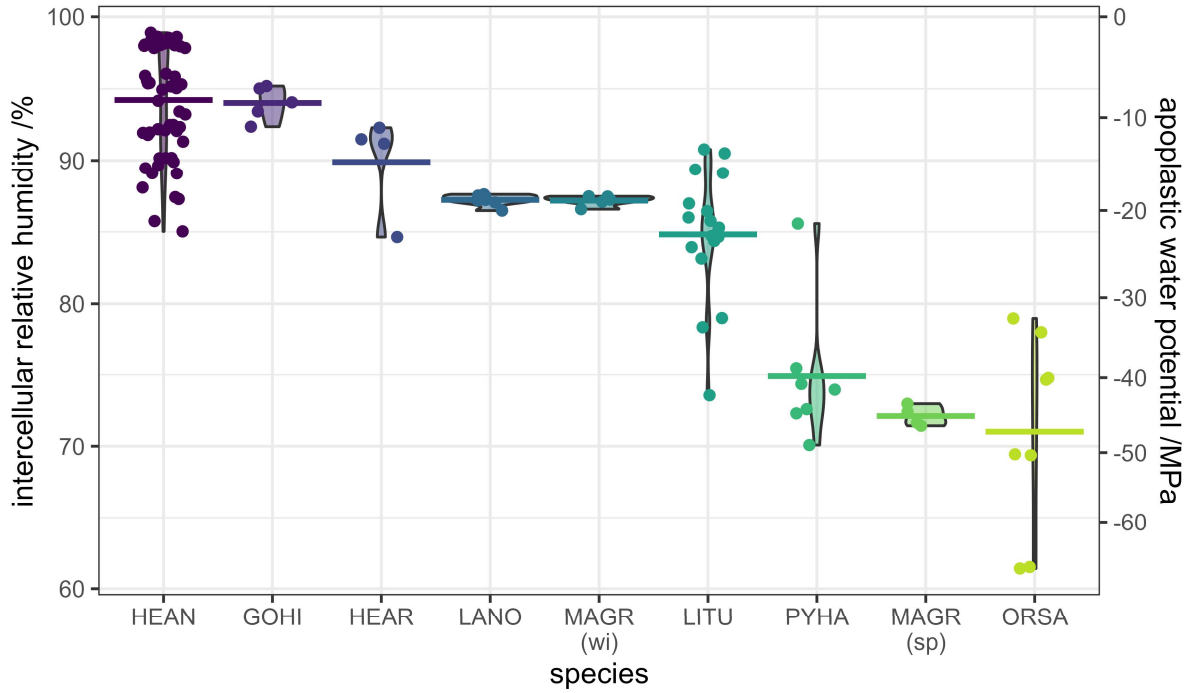

Figure 3. Distribution of intercellular relative humidity (left y-axis) and the equivalent water potential of apoplastic liquid water at the evaporating site (right y-axis) within and across species (HEAN: *Helianthus annuus*; GOHI: *Gossypium hirsutum*; HEAR: *Heteromeles arbutifolia*; LANO: *Laurus nobilis*; MAGR: *Magnolia grandiflora* [wi: winter (January 2026); sp: spring (May 2025)]; LITU: *Liriodendron tulipifera*; PYHA: *Pyrrosia hastata*; ORSA: *Oryza sativa*). Symbols are results from individual nitox-helox switches (i.e., technical replicates) and colored lines are within-species means. Details of individual experiments are given in Table 2. Mean intercellular relative humidity was significantly below zero for each species (and for each of MAGR [wi] and MAGR [sp]) ($p < 0.001$ except HEAR [$p = 0.0016$] and GOHI [$p = 0.0018$]).

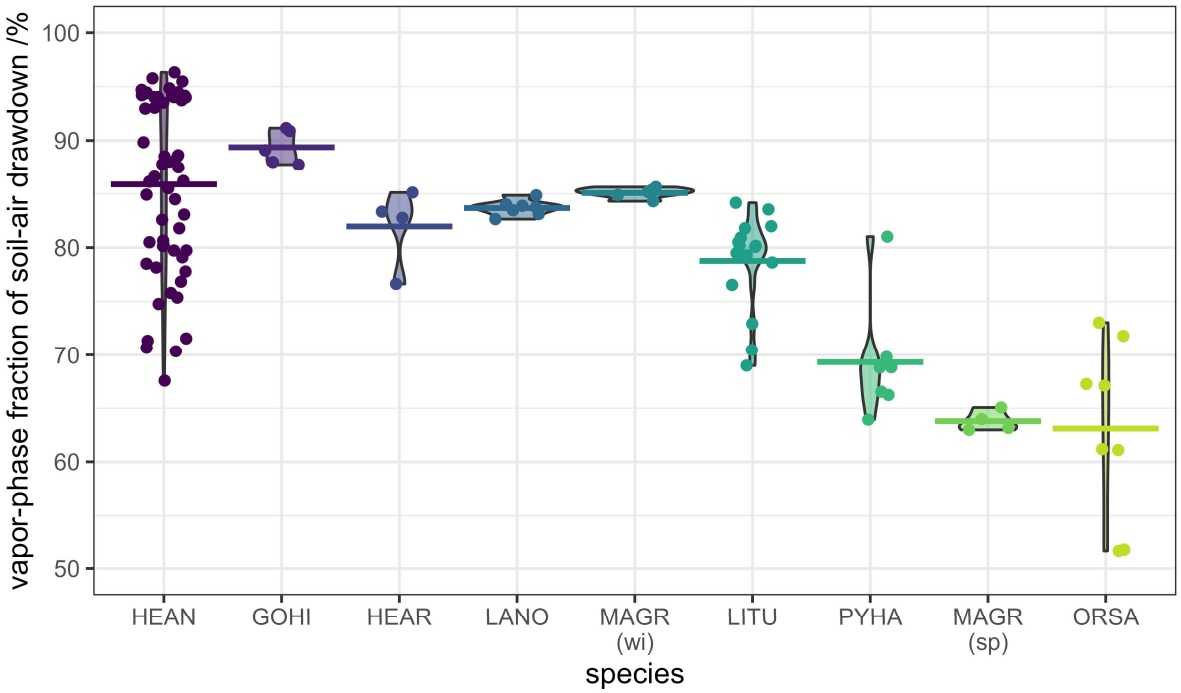

Figure 4. Vapor-phase fraction of total drawdown from saturation to ambient, across species (HEAN: *Helianthus annuus*; GOHI: *Gossypium hirsutum*; HEAR: *Heteromeles arbutifolia*; LANO: *Laurus nobilis*; MAGR: *Magnolia grandiflora* [wi: winter (January 2026); sp: spring (May 2025)]; LITU: *Liriodendron tulipifera*; PYHA: *Pyrrosia hastata*; ORSA: *Oryza sativa*). Symbols are results from individual nitox-helox switches (i.e., technical replicates) and colored lines are within-species means. Details of individual experiments are given in Table 2.

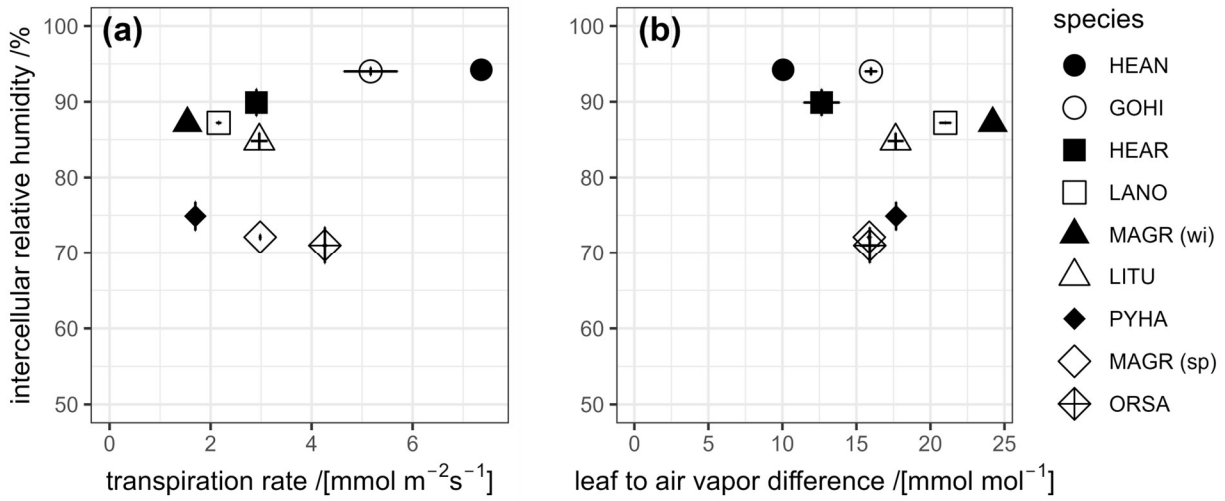

819
820
821 **Figure 5.** Intercellular relative humidity (*h*) was not related to (a) transpiration rate, *E*, or (b) leaf-to-air
822 water vapor mole fraction difference, Δw (the equivalent vapor pressure gradient [VPD_{leaf}] in kPa is
823 $\Delta w/10$), across species (error bars are ± SE). (HEAN: *Helianthus annuus*; GOHI: *Gossypium hirsutum*;
824 HEAR: *Heteromeles arbutifolia*; LANO: *Laurus nobilis*; MAGR: *Magnolia grandiflora* [wi: winter (January
825 2026); sp: spring (May 2025)]; LITU: *Liriodendron tulipifera*; PYHA: *Pyrrosia hastata*; ORSA: *Oryza sativa*).
826 Neither relationship shown is statistically significant (*h* vs *E*: $p = 0.284$; *h* vs Δw: $p = 0.674$). Details of
827 individual experiments are given in Table 2.
828

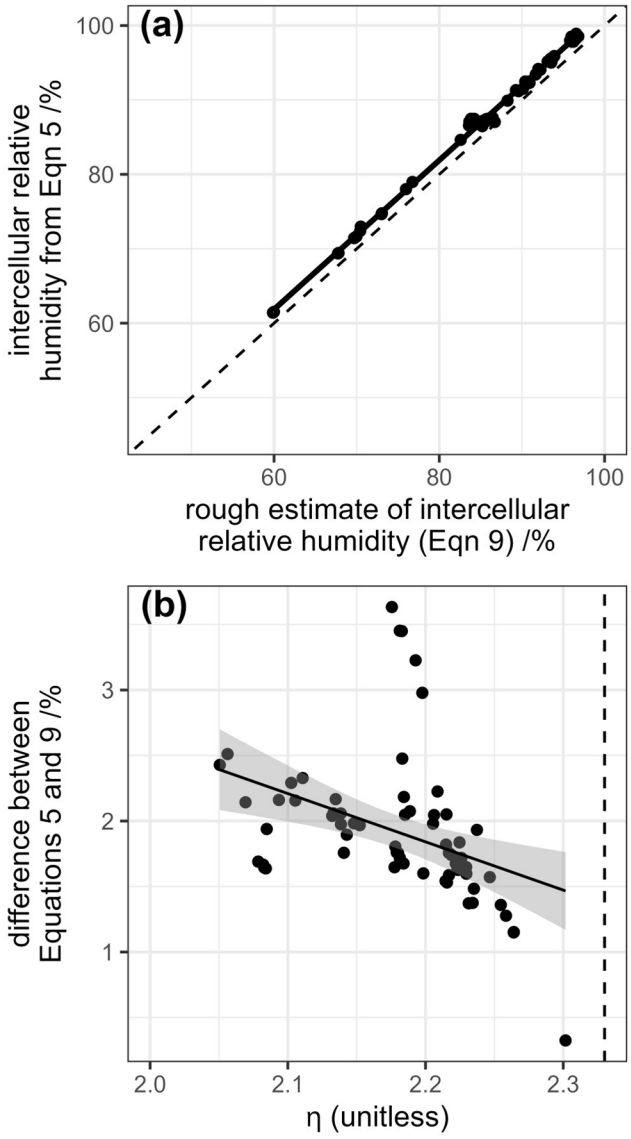

Figure 6. (a) Comparison of approximate solution ("rough estimate") of intercellular relative humidity (Eqn 9) with full solution (Eqn 5), and (b) relationship of the difference between those two estimates and the value of η (the proportion by which helox increases total vapor conductance). In (a), the dashed line is 1:1, and the solid line is a linear fit ($y = 1.007 \cdot x + 0.007$; $r^2_{adj} = 0.9943$, $p < 2.2 \cdot 10^{-16}$). In (b), the dashed vertical line is at $\eta = 2.33$ (the theoretical value in the limit of zero boundary layer resistance and zero cuticular conductance), and the solid line is a linear fit ($y = -0.065 \cdot \eta + 0.009$; $r^2_{adj} = 0.329$, $p < 0.001$).

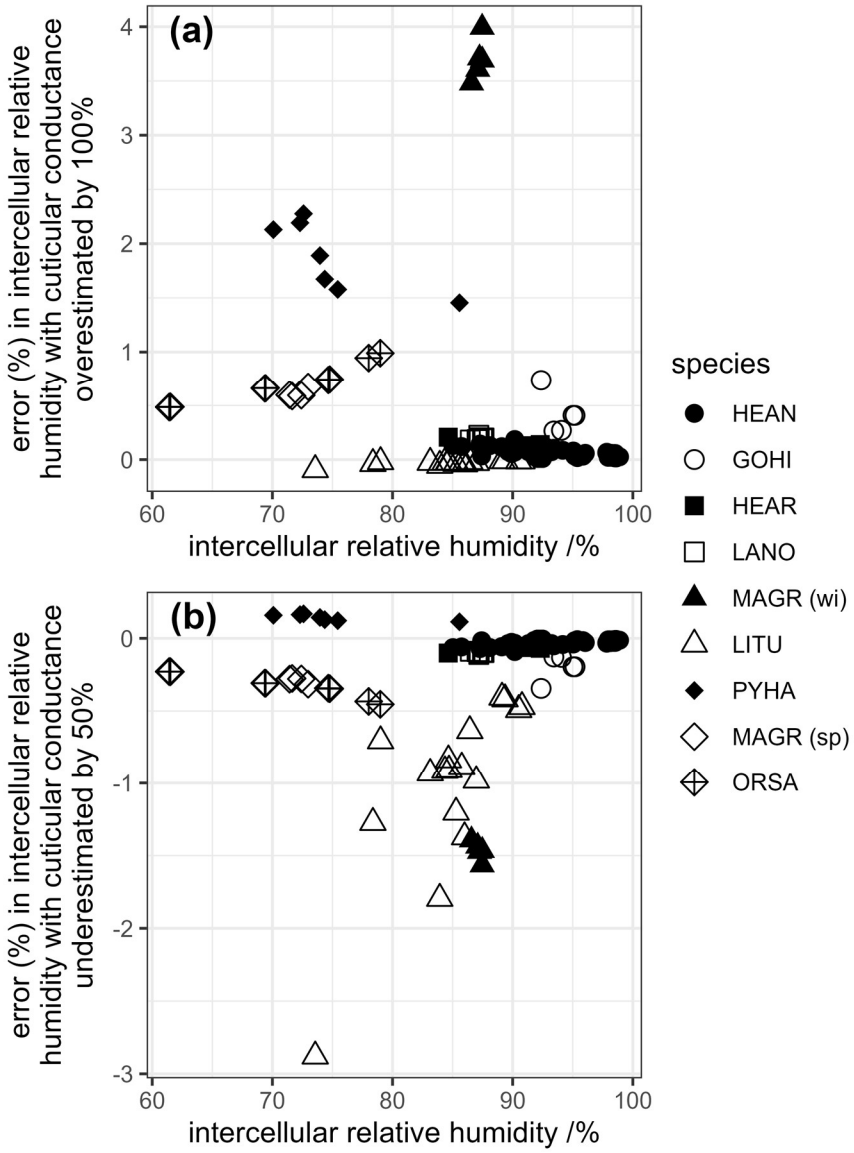

Figure 7. Potential error in estimation of intercellular relative humidity arising from uncertainty in the cuticular conductance (g_{cw}), for (a) 100% overestimation of the true value of g_{cw}, and (b) 50% underestimation of the true value of g_{cw}. (HEAN: *Helianthus annuus*; GOHI: *Gossypium hirsutum*; HEAR: *Heteromeles arbutifolia*; LANO: *Laurus nobilis*; MAGR: *Magnolia grandiflora* [wi: winter (January 2026); sp: spring (May 2025)]; LITU: *Liriodendron tulipifera*; PYHA: *Pyrrosia hastata*; ORSA: *Oryza sativa*.)